

p-Version Mesh Generation Issues

Xiao-Juan Luo, Mark S. Shephard, Jean-François Remacle
Scientific Computation Research Center, Rensselaer Polytechnic Institute, Troy, NY 12810,
xluo@scorec.rpi.edu, shephard@scorec.rpi.edu, remacle@scorec.rpi.edu

Robert M. O'Bara, Mark W. Beall
Simmetrix, Inc., Clifton park, NY 12065
obara@simmetrix.com, mbeall@simmetrix.com

Barna Szabó
Washington University, St. Louis, MO 63130
szabo@me.wustl.edu

Ricardo Actis
Engineering Software Research and Development, Inc., St. Louis, Missouri
ricardo@esrd.com

ABSTRACT

Higher order (p-version) finite element methods have been shown to be clearly superior to low order finite element methods when properly applied. However, realization of the full benefits of p-version finite elements for general 3-D geometries requires the careful construction and control of the mesh. A 2-D elasticity problem with curved boundary is used to clearly illustrate the influence of the mesh shape geometric approximation order and shape representation method on the accuracy of finite element solution in a p-version analysis. Consideration is then given to a new approach for the representation of mesh geometry for p-version meshes and to the automatic generation of p-version meshes.

Keywords: geometric approximation, Bezier polynomials, curvilinear mesh

1. INTRODUCTION

High order (p-version) finite element methods, characterized by the capability of exponential rate of convergence, are gaining popularity in industry. The basic functions of p-version finite elements, their convergence properties and aspects of their computer implementation have received extensive consideration in the literature (e.g. [1,3,10,16,17,18]). However, the critical technical issues of the appropriate geometric representation of p-version finite elements for solving partial differential equations over general three dimensional domains have not received adequate consideration. This paper first demonstrates that the accuracy of finite element solutions is strongly influenced by how well the geometry is approximated. Consideration is then given to a set of procedures being developed for proper generation of curved elements for p-version analyses.

Section 2 outlines the advantages of p-version finite elements assuming the proper choice of meshing and mapping procedures as required to preserve the superior rates of convergence. Section 3 examines the role of the mesh geometric approximation on the accuracy of the results obtained in terms of a specific curved domain problem with a known exact solution. This simple example clearly demonstrates that the use of quadratic geometric approximations for p-version finite elements does not lead to satisfactory solution results, in the sense that using p-lev-

els greater than 3 or 4 will produce results that are affected by the errors in mapping.

The requirements of Section 2 and results of Section 3 demonstrate the need for new mesh generation technologies to support p-version finite elements. Section 4 overviews current efforts on the development of such a mesh generation capability. Central to this new approach is the use of Bezier basis for the geometric representation of the element shapes. This basis allows one to effectively increase the order of geometric approximation in an efficient manner to any order desired. In addition, this basis supports effective methods for the execution of key operations such as determining the validity of curved finite elements and determining which mesh entities require shape change to make an invalid element valid.

2. p-VERSION FINITE ELEMENT MESHES

A finite element mesh serves two purposes: First, to allow representation of an arbitrary body by a collection of elements on which piecewise polynomial functions (occasionally augmented by other functions) are defined, and second, to control the error of approximation in terms of the data of interest.

The error of approximation depends on the finite element mesh and the polynomial degree of elements. In conventional FEA codes, the polynomial degree of elements are

fixed at 1 or 2, and the error is controlled by making sufficiently fine meshes: The diameter of the largest element is denoted by h . The errors of approximation are reduced as h is reduced. The term h -version refers to this approach. Since the mid-1980's an alternative, known as the p -version, matured sufficiently for use in professional practice. In this approach the primary role of the mesh is to represent the topological and geometric description of the object being modeled by a collection of elements and the error is controlled by the polynomial degree of elements, denoted by p . The error is reduced as p is increased. The p -version has certain advantages, which include faster rates of convergence and the ability to produce a sequence of solutions, corresponding to increasing p , automatically and without the need to alter the finite element mesh (so long as the mesh provides a satisfactory geometric approximation to the domain). This allows monitoring the convergence of the data of interest and estimating the errors of approximation. A large number of papers are available on this subject, see, for example, references [1,10,11,12,13,14].

The p -version poses certain new requirements for meshing. Since the size of elements is much larger than in the h -version, it is essential to use advanced mapping procedures so that the domain geometry is properly represented and integrated. Various procedures have been developed and implemented using special collocation points, known as the Babuska points, in connection with blending function techniques see, for example, references [2,7]. A typical finite element mesh used in the p -version is shown in Figure 1. The solution, representing the von Mises stress contours, was obtained with StressCheck[†].

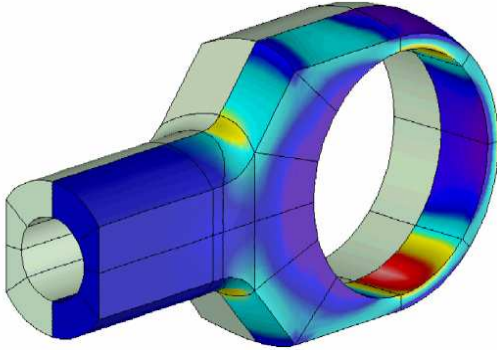


Figure 1. A typical finite element mesh in the p -version.

The proper choice of the mesh topological and geometric representation depends on the goals of computation. In solid mechanics the goals of computation are: (a) to determine stiffness characteristics of a structure, including natural frequencies; (b) to determine the strength characteristics, including stress maxima and stress intensity factors, and (c) to determine stability limits (buckling loads). In stiffness and stability computations it is generally possible to simplify meshing by omitting small features, such as fillets, bosses, small holes, etc. In strength computations,

when the goal is to compute the maximal stress, it is necessary to include fillets and all relevant features at least within the region where the maximal stress is sought. This is known as the region of primary interest. A frequent conceptual error in finite element analysis is reporting stresses in regions where the fillets and other small features were omitted.

The error of approximation has two sources: the local error and the pollution error. The pollution error, associated with the region of secondary interest, is controlled by ensuring that the error in the natural norm of the formulation, usually the energy norm, is sufficiently small. The local error, associated with the region of primary interest, depends on the local discretization (choice of mesh, mapping and the polynomial degree). This error is most efficiently controlled by the p -version of the finite element method.

3. INFLUENCE OF GEOMETRIC APPROXIMATION

This section discusses the influence of geometric approximation on the solution accuracy of p -version finite element method by using a benchmark two-dimensional elasticity problem for which analytic expressions for the exact displacement and stress field are known.

3.1 Model problem

An infinite plane weakened by an elliptical hole is deformed by the application of uniform tensile stress in the vertical direction at infinity as shown in Figure 2a. The relevant geometric parameters are the major axis a and minor axis b of the inner ellipse. These parameters are typically related to a third parameter, m , as

$$a = 1 + m, b = 1 - m, 0 \leq m < 1 \quad (1)$$

where $m = 0$ corresponds to a circle and $m = 1$ is a sharp crack.

Due to the double symmetry of the problem, only one quarter of the sub-domain ABCDE needs to be investigated as shown in Figure 2b. The exact stresses for the infinite domain problem are known along edges BC and DC and given by:

$$\sigma_x = \frac{1}{2}(S(1 - \cos 2\theta) + 2\tau_{\rho\rho} \cos 2\theta - 2\tau_{\rho\theta} \sin 2\theta) \quad (2)$$

$$\sigma_y = \frac{1}{2}(S(1 + \cos 2\theta) + 2\tau_{\rho\rho} \cos 2\theta + 2\tau_{\rho\theta} \sin 2\theta) \quad (3)$$

$$\sigma_{xy} = \frac{1}{2}((\tau_{\rho\rho} - \tau_{\theta\theta}) \sin 2\theta + 2\tau_{\rho\theta} \cos 2\theta) \quad (4)$$

where $S = \rho^4 - m^2 - 2m + 2\rho^2 \cos 2\theta$ and $\tau_{\rho\rho}$, $\tau_{\rho\theta}$ and $\tau_{\theta\theta}$ are the stress components expressed in elliptical coordinate system (ρ, θ) [15].

The mapping between Cartesian coordinate system (x, y) and elliptical coordinate system (ρ, θ) is

[†] StressCheck® is a trademark of Engineering Software Research and Development, Inc., St. Louis, Missouri

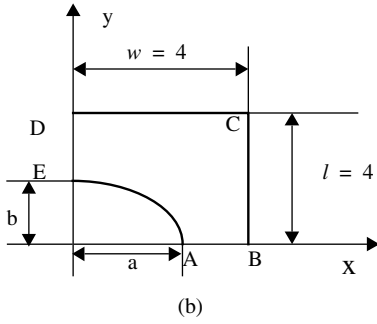
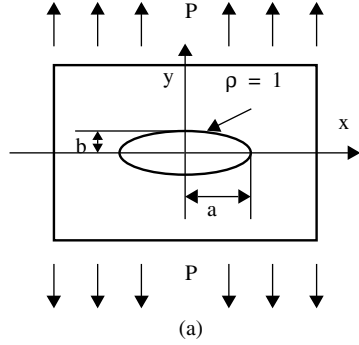


Figure 2. Elliptical hole in an infinite plane under the uniform tensile stress at infinity

$$x = R\left(\rho + \frac{m}{\rho}\right)\cos\theta, \quad y = R\left(\rho - \frac{m}{\rho}\right)\sin\theta, \quad R = \frac{a+b}{2}$$

Traction (Neumann) boundary conditions are applied on edges BC and CD and symmetric Dirichlet boundary conditions are imposed on edges DE and AB.

3.2 Maximum stress and strain energy

The maximum stress σ_{max}^{exact} of this problem is concentrated at vertex A and is a function of ratio a/b only, being defined as $\sigma_{max}^{exact} = 1 + 2a/b$. The finite element stress is computed directly in this study by computing the strains from the displacement solution then applying the appropriate isotropic material stress-strain relationship. Search for the maximum computed stress σ_{max}^{fem} is conducted over not only Gauss Quadrature points but also the vertices of each element [12]. The relative error in maximum stress defined as

$$\epsilon_{\infty} = \frac{\sigma_{max}^{fem} - \sigma_{max}^{exact}}{\sigma_{max}^{exact}} \times 100\% \quad (5)$$

is of great engineering interest.

The exact potential energy, Π^{exact} , of the sub-domain loaded by traction only without body force can be computed as

$$\begin{aligned} \Pi^{exact} &= -\oint (T_n u_n + T_t u_t) ds \quad (6) \\ &= -\left[\int_B^C (T_n u_n + T_t u_t) ds + \int_C^D (T_n u_n + T_t u_t) ds \right] \end{aligned}$$

Where T_n, T_t and u_n, u_t are normal and tangential traction components and displacement components respectively [12]. The angle α measured from the positive x axis to the normal of boundaries BC and CD are $0^0, 90^0$, so Eq. (6) can be simplified as

$$\Pi^{exact} = -\left[\int_B^C (u_x \sigma_x + u_y \tau_{xy}) dy + \int_C^D (u_y \sigma_y + u_x \tau_{xy}) dx \right] \quad (7)$$

where $\sigma_x, \sigma_y, \tau_{xy}$ are stress tensor components and u_x, u_y are displacement components [4]. The exact potential energy is obtained by numerically solving Eq. (7) to an accuracy substantially greater than any of the finite element solutions. The finite element potential energy Π^{fem} is computed by evaluating the product of load vector and finite element solution over the boundary. The relative error in energy norm is defined as

$$\|\epsilon\| = \sqrt{\left| \frac{\Pi^{exact} - \Pi^{fem}}{\Pi^{exact}} \right|} \times 100\% \quad (8)$$

3.3 Finite element meshes and geometric approximation shapes

A parameter $m = 0.25$ is selected to construct the first test model. An isotropic material with Young's Module of 1.0 and Poisson's ratio of 0.3 is used under the assumption of plane strain. The stress applied at the infinite boundary is 1.0. Table 1 provides the exact potential energy (to 7 digits significant figures) and the exact stress.

Table 1: Test problem

m	a	b	a/b	σ_{max}^{exact}	Π^{exact}
0.25	1.25	0.75	1.667	13/3	-7.8462131

The finite element method used for solving the problem consists of a double discretization. First, a mesh is introduced in order to discretize the geometrical domain. Then, the solution function space is approximated by a finite dimensional function space. Both geometrical and function space approximations introduce discretizations errors into the solution. In this work, we use polynomials for both discretizations where p represents the polynomial order for function space discretization and q represents the polynomial order for geometrical discretization.

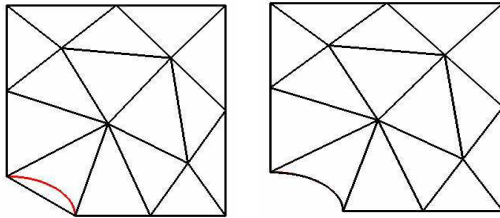
The discretization error of the finite element method can be written as the sum of two contributions:

$$E^{fem} = E_p^{fem} + E_q^{fem} \quad (9)$$

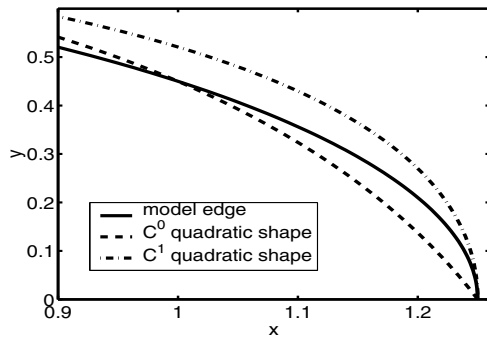
where E_q^{fem} is the geometrical error and E_p^{fem} is the func-

tional error. Studies of the convergence and accuracy of the finite element method for domains where geometrical error, E_q^{fem} , is identically zero or carefully controlled to be small, thus allowing study of the functional error, E_p^{fem} , are common. We investigate the total error when the geometrical discretization error, E_q^{fem} , contribution can be significant. In this study a coarse mesh with only one edge classified on the ellipse AE (see Figure 3) is used to perform the analysis and function polynomial orders from $p = 2$ to $p = 10$ are used and geometric polynomial orders from $q = 1$ to $q = 4$ are used. (A more complete study including additional mesh configuration and geometric approximation details is in preparation for publication [4])

For the mesh edge that is used to geometrically discretize the ellipse, linear ($q=1$), quadratic ($q=2$), cubic ($q=3$) and quartic ($q=4$) geometric approximations are selected. Two different fitting methods are applied for the $q>1$ cases. The first is a C^0 interpolant where the interpolating points are equally spaced in the parametric space of the edge. The second enforces C^1 continuity at the vertices A and E (see [4] for specifics on the construction of those geometric approximations). Close-ups of the geometric approximations in the vicinity of vertex A are shown in Figure 4.

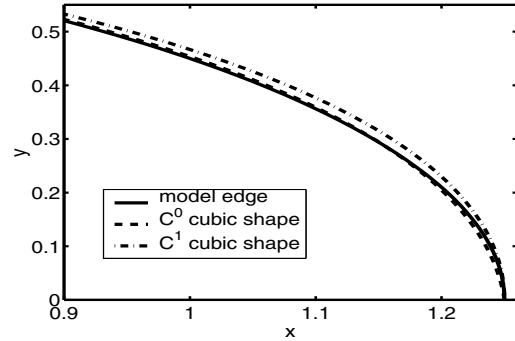


(a) Linear mesh (b) C^0 quartic mesh
Figure 3. Linear and C^0 quartic meshes

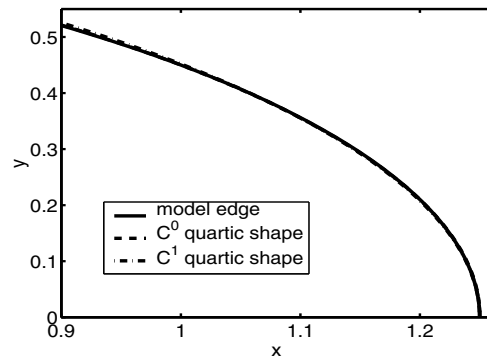


(a) C^0 and C^1 quadratic approximation shapes

Figure 4. Different geometric approximation shapes



(b) C^0 and C^1 cubic approximation shapes



(c) C^0 and C^1 quartic approximation shapes

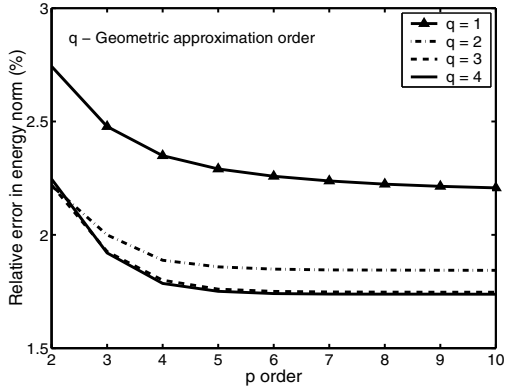
Figure 4. Different geometric approximation shapes

3.4 Result analysis

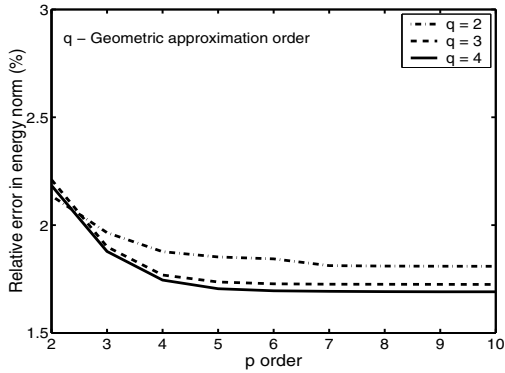
Convergence curves for the relative error in energy norm with respect to polynomial order p for the various geometric approximation orders q are shown in Figure 5. When the polynomial order increases past the geometric approximation order, the error in mapping begins to dominate the solution which is consistent with the basic theory [3]. The discretization error approaches a limit as p increases. This limit is essentially the E_q^{fem} because for very high p we solve the PDE nearly exactly on an approximated geometrical domain. The geometrical error E_q^{fem} is less when the geometric approximation order increases.

The performance of the different geometric approximations on the L^∞ norm of the maximum stress is a bit more complex. Figure 6a shows the relative error in maximum stress for the C^0 geometric approximations and Figure 6b shows it for the C^1 geometric approximations. For $q = 1$ (which is C^0) the computed maximum stress is underestimated at $p = 1$, but quickly increases past the exact value to overestimate the exact value by relative error of 122% at $p = 10$. Such behavior is expected since as p increases we are moving toward the solution of a problem with a sharp corner at point A where the stress theoretically goes to infinity. As q is increased for the C^0 case the sharp-

ness of the slope discontinuity at vertex A is decreased and the stress results become more accurate. However, it is interesting to note that in the case of the quadratic C^0 geometric approximation the stress is overpredicted by 45%, this is because the curved edge is not perpendicular to the symmetry plane due to the error in mapping.



(a) Relative error in energy norm for C^0 shapes

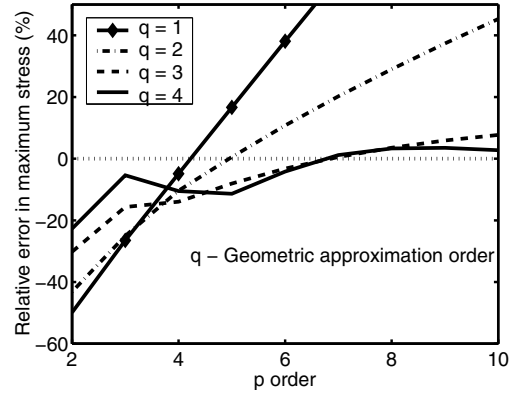


(b) Relative error in energy norm for C^1 shapes

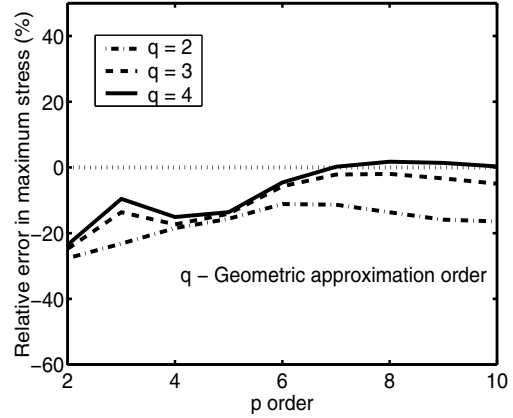
Figure 5. Relative error in energy norm of different p, q

A comparison of the C^0 and C^1 geometric approximations cases indicates that they underestimate the exact value for low order p . In the case of the C^0 geometric approximations the stress becomes overestimated when p continues to increase. In the case of the C^1 geometric approximations the stress is always underestimated for $q = 2$ and $q = 3$ while the $q = 4$ does slightly overestimate the value for high p . Figure 7 provides a more direct comparison of the C^0 and C^1 cases for the various geometric orders.

It should be noted that the geometric approximation error for the quadratic geometric approximations, $q = 2$, at $p = 10$ are substantial with an overestimate of 45% for the C^0 case and underestimate of 16% for the C^1 case. The cubic geometric approximations, $q = 3$, yield a smaller error at $p = 10$ with an overestimate of 7.7% for



(a) C^0 interpolation shape



(b) C^1 continuous shape

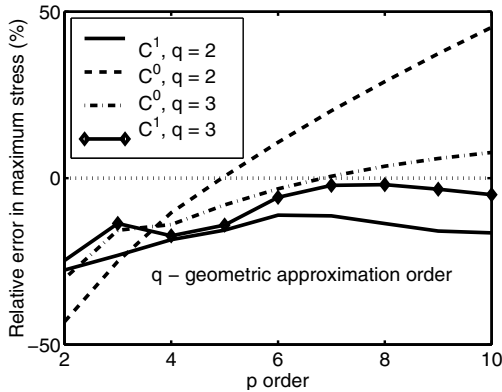
Figure 6. The convergence curve of relative error in maximum stress for different shapes

the C^0 case and underestimate of 5.0% for the C^1 case. The quartic geometric approximations, $q = 4$, yield the smallest error at $p = 10$ with an overestimate of 2.8% for the C^0 case and 0.29% for the C^1 case. These results are consistent with those presented in reference [15] where the ellipse geometry was approximated using a blending function method.

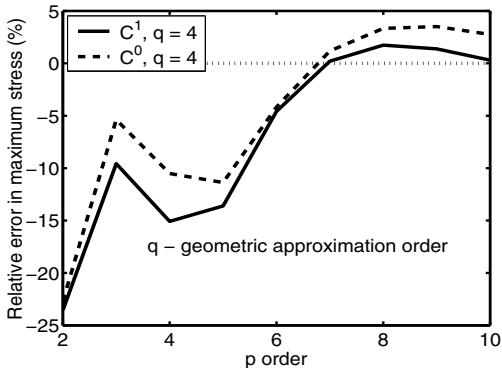
Although the results of C^0 geometric approximation shape indicate that appropriate combination of p and q will result in nearly 0% error for maximum stress such as $p = 5, q = 2$ and $p = 7, q = 3$ or 4 , the theoretical aspects of the optimal combination of p, q is still unclear and need further investigation. But it is important to notice that conventional assumption of quadratic geometric approximation for p-version finite element is not satisfied when the element polynomial order $p \geq 3$.

4. CURVILINEAR MESH GENERATION

This section overviews the curvilinear mesh generation



(a) Convergence curve for $q = 2, 3$



(b) Convergence curve for $q = 4$

Figure 7. Convergence curve for C^0 and C^1 shapes

procedure which starts with an initial linear mesh. The current development efforts are aimed at the effective representation and definition of meshes consisting of mixed geometric order elements as shown in Figure 8.

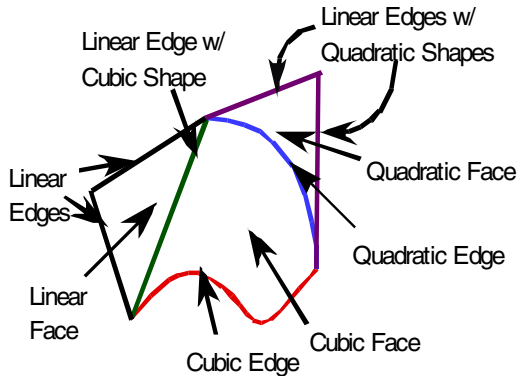


Figure 8. Example of mesh entities composed of different polynomial orders

In the mesh curving procedure, all of the mesh entities classified on the curved model boundaries are put into a list

with the attachment of a proposed geometric shape computed based either on interpolation or on approximation. The process will traverse the list and deal with one entity retrieved from it every step by checking the possibility to move the mesh entity to its proposed shape. If such shape movement does not cause any invalidities in the resulting mesh, the entity will be removed from the list. Otherwise, efforts involving geometric shape manipulation and local mesh modification operations such as splitting, swapping and collapsing are tried to eliminate the invalidities. The procedure continues till the list is empty.

Key techniques in the mesh curving procedure are

- Mesh entity geometric shape representation
- Curved mesh entity validity determination and invalidity correction
- Geometric shape optimization

The following subsections will discuss these issues.

4.1 Representing Mesh Shape

One approach to define the geometric shape of the mesh entities is to assign the same geometry as the portion of the model they classified on. However, the high computational cost of this method makes it undesirable. The alternative is to assign the mesh entity an appropriate geometric form. Interpolants such as Lagrange polynomials and approximations such as Bezier polynomial are possibilities. In the current work Bezier representations [5,6] are being used to define the mesh geometry instead of the more standard Lagrange interpolations due to the following properties of Bezier polynomials:

- Convex Hull Property: A Bezier curve, surface, or volume is contained in the convex hull formed by its control points.
- Variation Diminishing Property: An infinite plane can not intersect a Bezier curve more times than it intersects control polygon which allows more efficient intersection calculations.
- All derivatives and products of Bezier functions are easily computed Bezier functions.
- Computationally efficient algorithms for degree elevation and subdivision are available. These can be used to refine the shape's convex hull as well as adaptively refine the mesh's shape.

4.2 Determining Shape Validity

Previous implementations only tested the validity of mesh regions at the integration sites that were to be used in performing the analysis. Although this approach is sufficient for analysis in which the element shape, order and integration rule are fixed, it suffers from the following drawbacks:

- If the analysis changes the integration rule then the integration locations will change. As a result a region that was considered valid may suddenly become invalid. The only way to use this approach would be to test each region with respect to all the possible integration sites which can be a large number of evaluations when the polynomial order of the element can be increased.
- The test itself does not provide insight on how the region can be made valid either by changing the region's topology or its geometry.

- The test only focused on mesh regions. If a mesh edge or face were invalid (due to self-intersection) then all regions using it as part of its boundaries would also be invalid. Identifying and correcting these lower dimension mesh entities would effectively reduce the number of invalid mesh regions that need to be corrected.

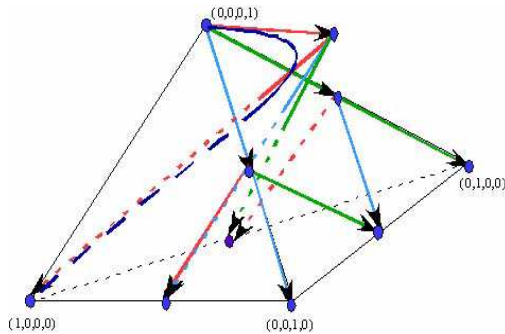
A new approach that builds on the Bezier properties to test the global validity of a mesh entity has been developed. In the case of a Bezier tetrahedron volume, the Jacobian $J(\xi)$ of the geometric mapping $\underline{x}(\xi)$ is

$$J(\xi) = \left| \frac{\partial \underline{x}}{\partial \xi_i} \right| \quad (10)$$

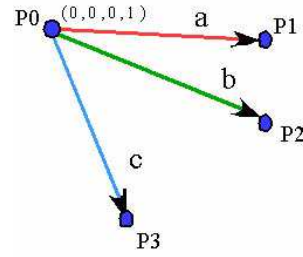
Where ξ represents the natural coordinates of the element. So the determinant of Jacobian $\det(J)$ is computed as

$$\det(J) = \left(\frac{\partial \underline{x}}{\partial \xi_0} \times \frac{\partial \underline{x}}{\partial \xi_1} \right) \cdot \frac{\partial \underline{x}}{\partial \xi_2} \quad (11)$$

$\frac{\partial \underline{x}}{\partial \xi_0}$, $\frac{\partial \underline{x}}{\partial \xi_1}$ and $\frac{\partial \underline{x}}{\partial \xi_2}$ are the three partial derivatives of $\underline{x}(\xi)$ which are Bezier functions. Because product of Bezier functions are also Bezier functions, the $\det(J)$ can be represented as a polynomial in Beizer form which is bounded by its convex hull of control points. If all of the control points of the $\det(J)$ are greater than zero then the region's $\det(J)$ must be greater than zero everywhere. The test works for any polynomial order. An invalid tetrahedron region determined by the above algorithm is shown in Figure 9. Where the placement of control point P_1 causes $a \cdot (b \times c) < 0$.



(a) An invalid Bezier tetrahedron region
Figure 9. Determination of invalid Bezier region



(b) Invalid tetrahedron region by moving P_1
Figure 9. Determination of invalid Bezier region

4.3 Correcting Invalid Mesh Entity

The validity test also provides information in the case of an invalid shape in terms of possible modifications that can be used to correct the shape. An invalid region can be corrected by shape manipulation and/or local mesh modifications using split, swap and collapse operations.

4.3.1 Correcting Invalidity by Shape Manipulation

Four possible solutions to correct the invalid region shown in Figure 9 by shape manipulation are presented in Figure 10 where the movement of control points P_0 , P_1 , P_2 and P_3 are to ensure that the third partial derivative vector coming to the control point P_0 always lies in the positive side of the plane defined by another two partial derivative vectors which makes $a \cdot (b \times c) > 0$ such that the region becomes valid.

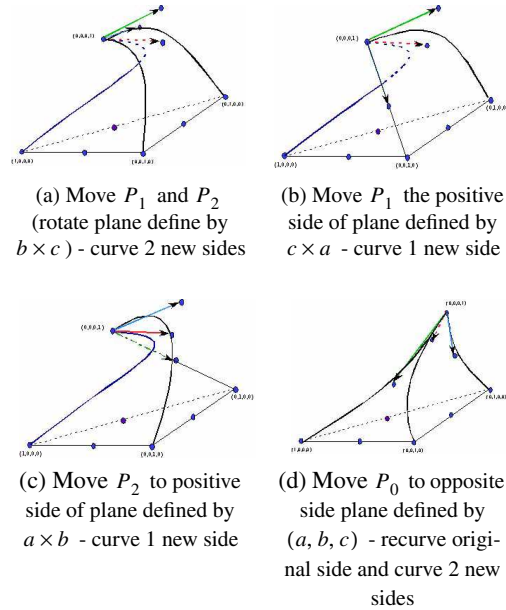


Figure 10. Correct invalid region by shape manipulating

Another example of shape manipulation is shown in Figure 11. The top image shows four mesh faces made invalid due to the curving of four mesh edges classified on the circular hole. The center image is a close up of one of the invalidities. One possible solution to this problem would be to curve each of the faces' remaining linear edges in order to resolve the invalidities. The result of these shape modifications are shown in the bottom image.

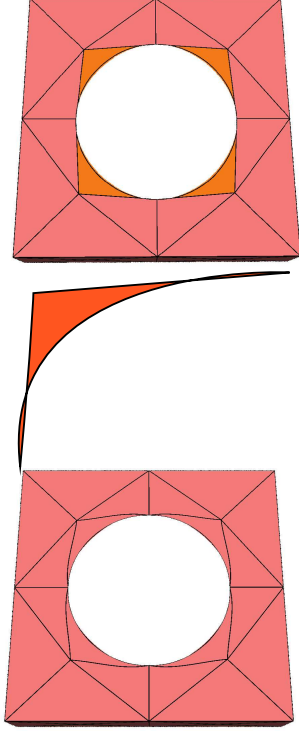


Figure 11. The effect of curving mesh edges classified on the planar face in order to correct the original highlighted invalid mesh faces

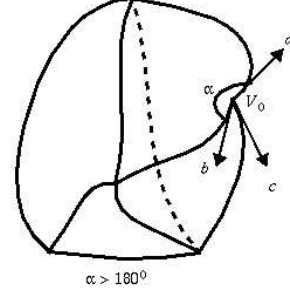
4.3.2 Correcting Invalidity by Curved Splitting

The split operation usually is chosen to fix an invalid region that at least an angle formed by two partial derivative vectors at its vertex is bigger than 180^0 , see Figure 12(a). New mesh edge(s) must be introduced through the vertex to refine the region in order to eliminate the invalidity shown in Figure 12(b).

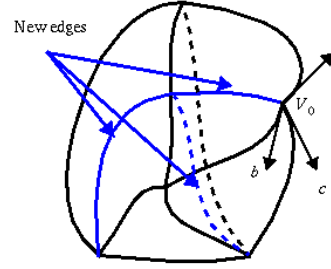
The Bezier split operation is implemented based on the assumption that the original curved entity shape remains unchanged up to any order in parametric space. The benefits for applying split operation are

- No topological validity determination required
- The geometric shapes of the new created mesh entities are well formulated.

For example, when splitting a n th order Bezier mesh tetrahedron region at location $\tilde{v}(v_1, v_2, v_3, v_4)$, the control points net of the new four regions can be computed as



(a) Invalidity at vertex V_0 because $\alpha > 180^0$



(b) Edge split to fix the region invalidity

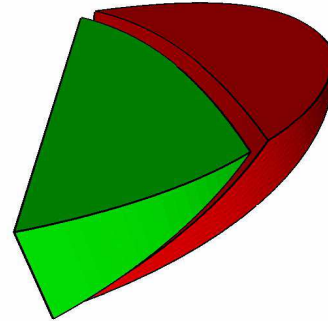
Figure 12. Splitting in mesh curving procedure

$$\hat{b}(r, j, k, l) = b_{j_0}^r(\tilde{v}), \hat{b}(j, r, k, l) = b_{j_1}^r(\tilde{v}) \quad (12)$$

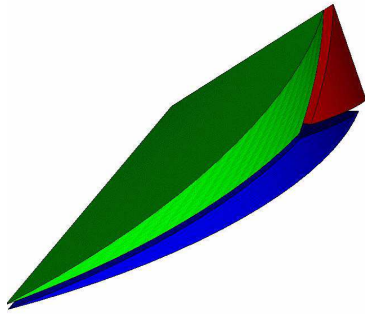
$$\hat{b}(j, k, r, l) = b_{j_2}^r(\tilde{v}), \hat{b}(j, k, l, r) = b_{j_3}^r(\tilde{v}) \quad (13)$$

where \tilde{v} is volume coordinates and $v_1 + v_2 + v_3 + v_4 = 1$. $j_0 = (0, j, k, l)$, $j_1 = (j, 0, k, l)$, $j_2 = (j, k, 0, l)$ and $j_3 = (j, k, l, 0)$. $b_{j_0}^r$, $b_{j_1}^r$, $b_{j_2}^r$ and $b_{j_3}^r$ are corresponding control points of original curved tetrahedron region.

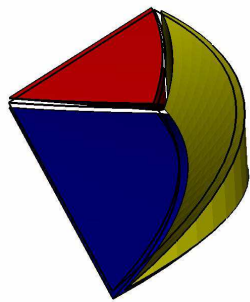
Bezier edge and face split operations are the special cases of region split where one or two parameters of \tilde{v} are equal to zero. Examples are shown in Figure 13.



(a) edge split - create two new curved regions
Figure 13. Bezier edge, face, region split operation



(b) face split - create three new curved regions

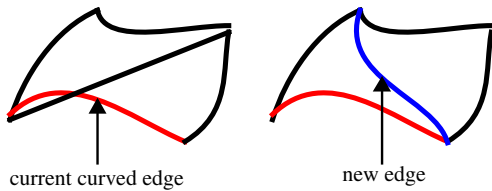


(c) region split - create four new curved regions

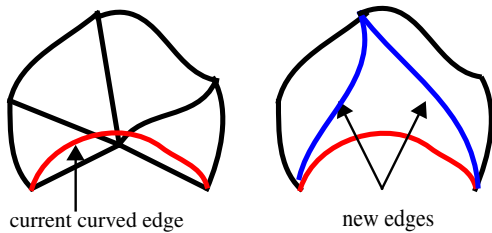
Figure 13. Bezier edge, face, region split operation

4.3.3 Correcting Invalidity by Curved Swapping and Collapsing

Curved edge swap and collapse operations can increase the space needed by the shape movement of the current curved mesh entity from the list. They are practical useful when the invalidities are caused by interferences, see Figure 14.



(a) Curved edge swap



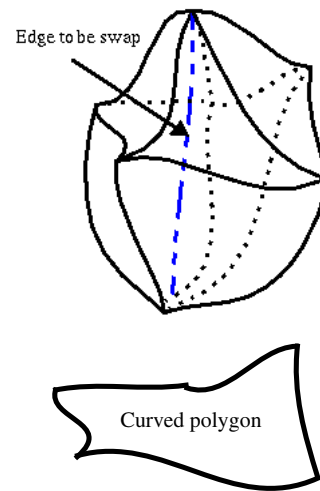
(b) Curved edge collapse

Figure 14. Curved edge swap and collapse

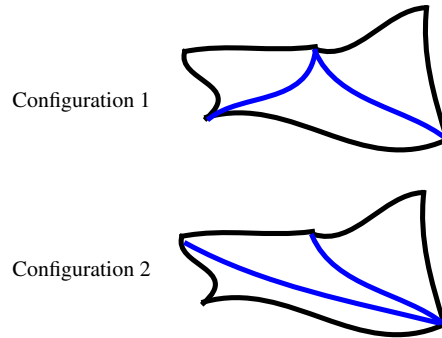
In swap and collapse operations, a curved polygon is created after deleting all of the higher bounded mesh entities connecting to the split and swap edge, see Figure 15 (a). Usually the edge number of the curved polygon is bigger than 4. There are two important issues affecting the operation application result,

- Appropriate topology configuration of the curved polygon
- Shape construction of the new edge(s) and face(s)

For example, two possible configurations and shape constructions for Figure 15(a) are presented in Figure 15(b). Both of them are topological and geometrical valid. However, solutions can not be similarly generalized in parametric space as split operation and are still under investigation and development.



(a) Curved polygon created by edge swap



(b) Two valid configuration for the curved polygon

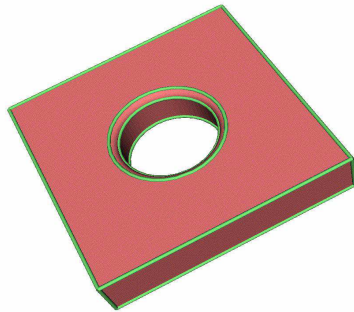
Figure 15. Configurations and shape construction of edge swap

4.3.4 Shape Quality of Curved Mesh

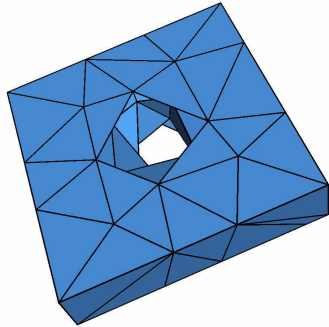
One important piece needed for curvilinear mesh generation that is not yet resolved is the aspect of mesh quality measures of curved mesh entities. Quality metrics are

important when choosing which mesh modification or configuration to apply in order to correct an invalid mesh shape. For example, another solution to the problem posed in Figure 11 is to relocate the faces' vertices opposite to curved edges. The definition of quality metrics for curved element should be guided to be directly related to the p-version finite element solution accuracy. Some investigation results of one example are presented below for the purpose to demonstrate that different selection of metrics measurement leads to different quality results and need carefully consideration.

Two curved meshes based on the same geometry model are presented in Figure 16. The first curvilinear mesh is created based on the criteria to maximize the minimum determinant of Jacobian of each region and the second curved mesh is constructed just by interpolating geometry model. Volume and normalized Δd_{max} - which is defined as the normalization of maximum distance variation between the mesh entities and the geometry model boundary they classified on to the longest diagonal edge length of the model domain - are used to compare these two meshes. Table 2 clearly shows that curved meshes (c) and (d) have better approximation quality to the geometry model comparing than linear mesh. But the difference between curved mesh (c) and (d) is small if volume is applied as the quality measure metric. But the normalized Δd_{max} for curved mesh (d) is better than that of mesh (c).

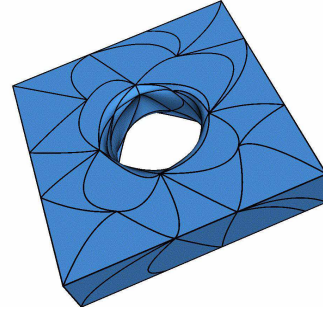


(a) geometry model

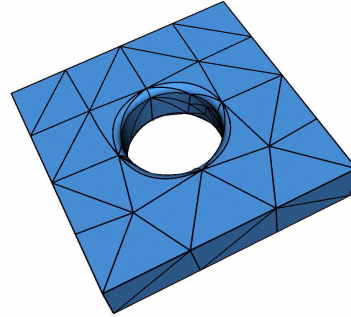


(b) Linear mesh

Figure 16. Different curvilinear meshes for the same geometry



(c) curvilinear mesh by maximize the minimum determinant of Jacobian of each region



(d) curvilinear mesh by geometry interpolation

Figure 16. Different curvilinear meshes for the same geometry

Table 2: Shape quality comparison

	Volume	Δd_{max}
Model	3.5412E-04	
Linear Mesh	3.7402E-04	8.65976%
Mesh (a)	3.5821E-04	2.93822%
Mesh (b)	3.5715E-04	0.19668%

4.4 Approximating the Model's Boundary

Another important issue is how to best approximate the model boundary. As previously discussed, the approximation error between the original geometric model and the mesh can have a strong impact on the analysis. Currently interpolation methods are used to "fit" the mesh boundary to the model boundary at certain sample points on the boundary; however, using traditional methods, such as chord length interpolation [9], can cause undesirable boundary artifacts. In polynomial surfaces that are beyond quadratic. One of the major issues is to find appropriate parametric locations for the interpolation points that are not on the edges of a triangular surface. Optimization techniques that improve the quality of the surface mesh by reducing these artifacts need to be investigated. An example is shown in Figure 17.

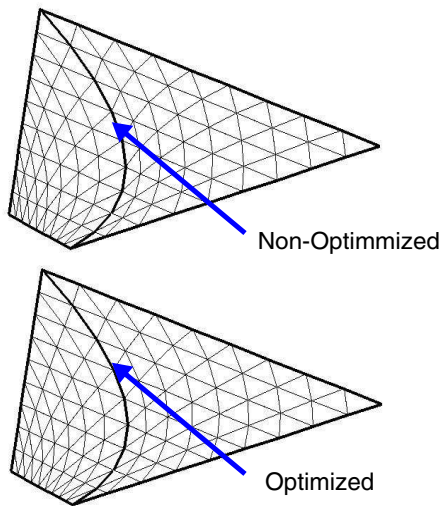


Figure 17. Comparison of non-optimized mesh faces with optimized mesh faces

Both meshes use the same edge interpolation points. However, the top image shows that the isoparametric lines through the common edge is really unsmooth. In the bottom image the isoparametric lines change smoothly after the optimization of face interpolation points.

As previously mentioned, in addition to basic interpolation approaches, constraints such as the order of geometric continuity between mesh entities need to be taken into consideration when meshing the boundary.

4.5 Preliminary Results

Figure 18 shows the result of generating a curved mesh of maximum polynomial degree $q = 3$ from a linear mesh. The boundary mesh entities' shapes have been optimized to reduce undesirable artifacts. Figure 19 shows a more complex example of curve mesh generation as well as the impact raising the polynomial degree on the boundary mesh. Double curvatures are clear shown in the cubic Bezier mesh to better approximate the geometry model.

Figure 20 shows the application of quadratic curving on models supplied by ESRD. Figure 21 shows a cubic curved mesh which involves shape manipulation and curved collapse operation to resolve the invalidities. The initial linear meshes show the desired coarseness of the meshes.

5. CLOSING REMARK

The p-version finite element method provides an effective method to apply simulation technologies in engineering design. However, as this paper has pointed out, the application of these methods requires the careful construction of the meshes and control of their geometric approximation to curved domains. The brief introduction to the methods currently under development to support p-version mesh generation indicate the need to address a number of issues that do not need to be considered when low order finite ele-

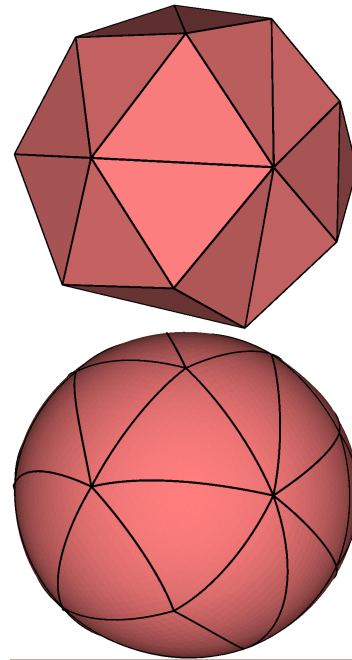


Figure 18. The result of curving a straight sided mesh classified on a sphere using a maximum polynomial degree of 3

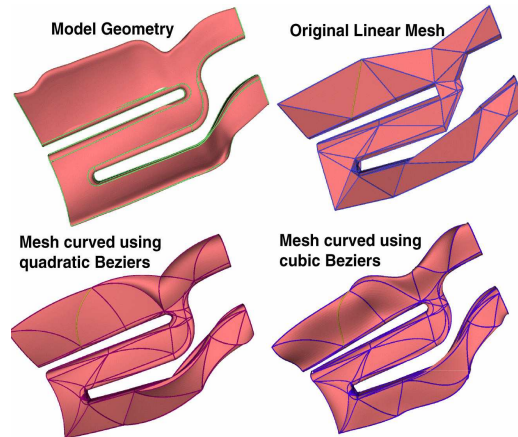


Figure 19. More complex curving example showing how the polynomial degree affects the shape of the highlighted mesh edge.

ments are to be used.

6. ACKNOWLEDGEMENTS

Aspects of this work are supported by the National Science Foundation (DMI-0132742) and the Office of Naval Research (N00014-99-0725).

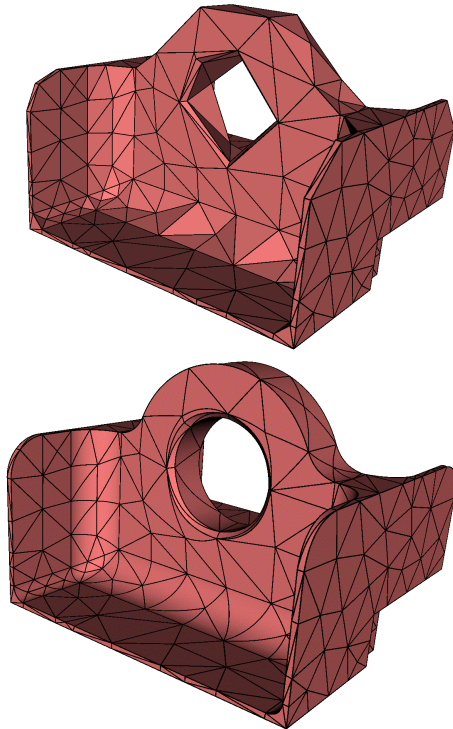


Figure 20. The application of Simmetrix's quadratic curving tool on a model supplied by ESRD.

7. REFERENCES

- [1] I. Babuska and B. Szabó, "Trends and New Problems in Finite Element Methods", *The Mathematics of Finite Elements and Applications*, J.R. Whiteman, Ed, John Wiley and Sons, Chichester, pp. 1-33 (1997)
- [2] Q. Chen and I. Babuska, "Approximate Optimal Points for Polynomial Interpolation of Real Functions in an Interval and in a Triangle", *Comput. Methods Appl. Mech. Engrg.*, Vol. 128, pp. 405-417 (1995).
- [3] S. Dey, M.S. Shephard and J.E. Flaherty, "Geometry-based issues associated with p-version finite element computations", *Comput., Methods. Appl. Mech. Engrg.*, Vol 150, pp. 39-55 (1997).
- [4] X.J. Luo, M.S. Shephard and J.F. Remacle, "The effect of geometric approximation for curved domains in p-version finite element method", in preparation.
- [5] G.E. Farin, *Curves and Surfaces for Computer Aided Geometric Design - A Practical Guide*, 3rd Edition. Boston: Academic Press, (1993).
- [6] R.T. Farouki and V.T. Rajan, "Algorithms for polynomials in Bernstein", *Comput. Aid. Geom. Des.*, Vol. 5, pp. 1-26 (1988).
- [7] G. Királyfalvi and B. Szabó, "Quasi-Regional Mapping for the p-Version of the Finite Element Method," *Finite Elements in Analysis and Design*, Vol. 27, pp. 85-97 (1997).
- [8] N.I. Muskhelishvili, *Some Basic Problems of the Mathematical Theory of Elasticity*, Groningen, P. Noordhoff, (1963).

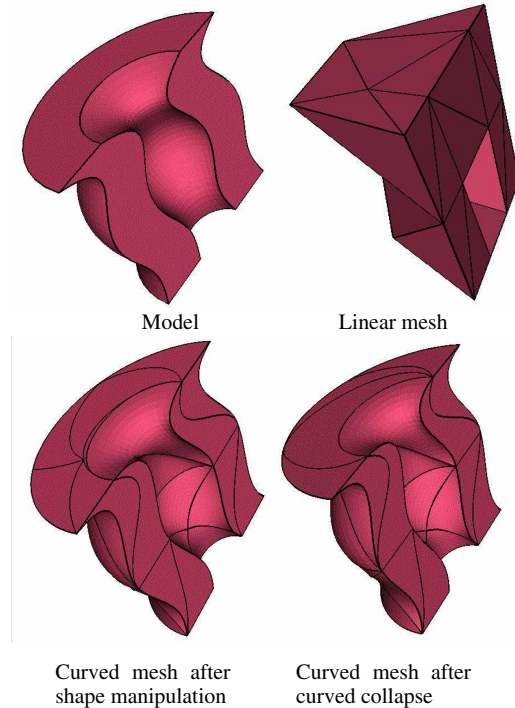


Figure 21. Example of a cubic curved mesh produced by applying shape manipulation and collapse operation

- [9] L. Piegl and W. Tiller, *The NURBS Book - 2nd Edition*, Berlin: Springer-Verlag (1997).
- [10] B. Szabó, "The p- and hp-Versions of the Finite Element Method in Solid Mechanics," *Comput. Methods. Appl. Mech. Engrg.*, Vol. 80, pp. 185-195 (1990).
- [11] B. Szabó, "On Reliability in Finite Element Computations", *Comp. & Structures*, Vol. 39, pp. 729-734 (1991).
- [12] B. Szabó and I. Babuska, *Finite Element Analysis*, John Wiley & Sons New York, (1991).
- [13] B. Szabó and R. Actis, "Finite Element Analysis in Professional Practice," *Comput. Methods. Appl. Mech. Engrg.*, Vol. 133, pp. 209-228 (1996).
- [14] B. Szabó, "Quality Assurance in the Numerical Simulation of Mechanical Systems," *Computational Mechanics for the 21st Century*, B.H.W. Topping, Ed., Saxe-Coburg Pub., Edinburgh pp.51-69, (2000).
- [15] Z. Yosibash and B. Szabó, "Convergence of Stress Maxima in Finite element Computations", *Comm. Numer. Methods Engrg.* Vol. 10: pp. 683-697, (1994).
- [16] I. Babuska and M. Suri, "The p and h-p versions of the finite element method, basic principles and properties", *SIAM J. Numer. Anal.*, Vol. 36(4) pp. 578-631 (1994).
- [17] P. Carnevall and R.B. Morris, Y. Tsuji and G. Taylor, "New basis functions and computational procedures of p-version finite element analysis," *Int. J. Numer. Methods. Engrg.*, Vol. 36 pp. 3759-3779 (1993).
- [18] C.G. Kim and M. Suri, "On the p-version of the finite element method in the presence of numerical integration", *Numer. Methods. Partial Differential Equations*, Vol. 9 pp. 593-629 (1993).